Redox Biology 64 (2023) 102804

Contents lists available at ScienceDirect

Redox Biology

journal homepage: www.elsevier.com/locate/redox

TMBIM6 deficiency leads to bone loss by accelerating osteoclastogenesis

Sun-Ju Yi [a], You-Jee Jang [b], Seokchan Lee [a], Sung-Jin Cho [a], Kyuho Kang [a], Jae-Il Park [c], Han-Jung Chae [d], Hyung-Ryong Kim [e,**], Kyunghwan Kim [a,*]

[a] Department of Biological Sciences and Biotechnology, Chungbuk National University, Cheongju, Chungbuk, 28644, Republic of Korea
[b] Department of Biomedical Laboratory Science, Honam University, Gwangju, Republic of Korea
[c] Korea Basic Science Institute, Gwangju Center at Chonnam National University, Gwangju, Republic of Korea
[d] School of Pharmacy and New Drug Development Research Institute, Jeonbuk National University, Jeonju, Republic of Korea
[e] Department of Pharmacology, College of Dentistry, Jeonbuk National University, Jeonju, Republic of Korea

ARTICLE INFO

Keywords:
TMBIM6
Bone development
Osteoclastogenesis
Reactive oxygen species
p65

ABSTRACT

TMBIM6 is an endoplasmic reticulum (ER) protein that modulates various physiological and pathological processes, including metabolism and cancer. However, its involvement in bone remodeling has not been investigated. In this study, we demonstrate that TMBIM6 serves as a crucial negative regulator of osteoclast differentiation, a process essential for bone remodeling. Our investigation of Tmbim6-knockout mice revealed an osteoporotic phenotype, and knockdown of Tmbim6 inhibited the formation of multinucleated tartrate-resistant acid phosphatase-positive cells, which are characteristic of osteoclasts. Transcriptome and immunoblot analyses uncovered that TMBIM6 exerts its inhibitory effect on osteoclastogenesis by scavenging reactive oxygen species and preventing p65 nuclear localization. Additionally, TMBIM6 depletion was found to promote p65 localization to osteoclast-related gene promoters. Notably, treatment with N-acetyl cysteine, an antioxidant, impeded the osteoclastogenesis induced by TMBIM6-depleted cells, supporting the role of TMBIM6 in redox regulation. Furthermore, we discovered that TMBIM6 controls redox regulation via NRF2 signaling pathways. Our findings establish TMBIM6 as a critical regulator of osteoclastogenesis and suggest its potential as a therapeutic target for the treatment of osteoporosis.

1. Introduction

Bones undergo continuous remodeling throughout life to maintain strength and mineral homeostasis. During bone remodeling, bone resorption is tightly coupled to bone formation; proper balance between bone resorption by osteoclasts and bone formation by osteoblasts is essential to maintain healthy bones. Excessive bone resorption leads to osteopenia and osteoporosis, whereas excessive bone formation leads to osteopetrosis [1–3].

Osteoclasts are responsible for bone resorption, which plays a pivotal role in beginning the bone remodeling cycle [4,5]. Osteoclast precursor (OCP) cells are differentiated from the monocyte-macrophage lineage cells derived from hematopoietic stem cells. OCP cells differentiate into osteoclasts upon stimulation by two key ligands, the macrophage colony-stimulating factor (M-CSF) and the receptor activator of nuclear factor kappa-B ligand (RANKL) [6,7]. Typically, the binding of RANKL to the receptor activator of nuclear factor kappa-B (RANK, also known as TNFRSF11a) activates nuclear factor kappa-B (NF-κB), activator protein 1 (AP-1), and nuclear factor-activated T cells c1 (NFATc1), which modulate the expression of osteoclast-specific genes, including tartrate-resistant acid phosphatase (TRAP), cathepsin K, osteoclast-associated receptor, and matrix metalloproteinase-9 (MMP-9) [8–14]. Recent studies have shown that the RANKL signaling stimulates the production of reactive oxygen species (ROS), which plays an important role in osteoclastogenesis [15–20].

Transmembrane BAX inhibitor motif-containing (TMBIM) 6 is a member of the TMBIM family that possesses antiapoptotic activity. The TMBIM family shares a domain containing six or seven transmembrane regions and is conserved among mammals, insects, fish, plants, viruses, and yeast [21]. TMBIM6 was originally identified as an inhibitor of BAX-induced apoptosis through functional screening in yeast [22]. Further studies found that TMBIM6 is a hydrophobic transmembrane protein exclusively present on the endoplasmic reticulum (ER), where it modulates ER stress, ROS accumulation, and Ca^{2+} concentration

* Corresponding author.
** Corresponding author.
E-mail address: kyungkim@chungbuk.ac.kr (K. Kim).

https://doi.org/10.1016/j.redox.2023.102804
Received 27 May 2023; Received in revised form 15 June 2023; Accepted 27 June 2023
Available online 28 June 2023

[23–28]. The role of TMBIM6 in cancer development and progression has also been investigated. The expression levels of TMBIM6 are upregulated in breast, glioma, prostate, uterine, and ovarian cancer but downregulated in stomach, colon, kidney, lung, and rectal cancer [28]. A recent study reported that TMBIM6 is associated with tumor growth and cancer-related signaling [29].

Several studies using knockout mice have investigated TMBIM6's physiopathological roles, conducted by both our colleagues and other research groups. TMBIM6-depleted mice showed increased ER stress-induced tissue damage [25,30], increased liver generation after partial hepatectomy [31], obesity in adulthood, and development of leukopenia and hepatic steatosis [31,32], impeded hepatic glucose metabolism and insulin signaling under high-fat diet conditions [33], greater testicular damage after cisplatin treatment [34], and ER stress response failure in aging [35]. Furthermore, Our recent studies have demonstrated that TMBIM6 participates in odontoblast differentiation [36] and also exhibits elevated expression levels in both osteoblasts and osteoclasts [37], suggesting its potential role in regulating bone remodeling. We have extended these observations by investigating the potential role of TMBIM6 in bone remodeling.

In this study, we present that *Tmbim6* knockout mice exhibit an osteoporotic phenotype. We demonstrate that TMBIM6 depletion significantly enhanced RANKL-mediated osteoclast differentiation in the mice. Our study also uncovers the role of TMBIM6 in negatively regulating the p65 signaling pathway by suppressing the production of reactive oxygen species. Additionally, we show that N-acetyl cysteine (NAC) treatment inhibits the osteoclastogenesis upregulation in TMBIM6-depleted cells. Finally, we identify TMBIM6 as a critical regulator of the NRF2 signaling pathways during osteoclast differentiation.

2. Materials and methods

2.1. Mice and micro-CT analysis

All procedures for mouse care were performed in accordance with the Institutional Animal Care and Use Committees of Chonbuk National University. For all experiments, the mice were on a C57BL/6J background and were housed in a mouse facility on a 12-h light/dark cycle in a 22 °C temperature-controlled room. The *Tmbim6* wild-type and knockout mice used in this study have been described previously [25]. Age-matched male mice were used for experiments.

The distal femur of 3-month-old male *Tmbim6* wild-type and knockout mice was subjected to micro-CT analysis using a Quantum GX micro-CT imaging system (PerkinElmer, Hopkinton, MA, USA) with the following parameters: 90 kV, 80 μA, and a 4-min scanning time. Images were acquired with a cubic voxel size of 20 μm, covering a field of view (FOV) of 10 mm × 10 mm. The region of interest (ROI) for trabecular bone was defined as the area located 1 mm from the growth plates, and 100 slices (2 mm) were reconstructed. The trabecular bone parameters were analyzed and calculated using the ROI tool in Analyze 12.0 software (AnalyzeDirect, Overland Park, KS, USA) [38].

2.2. Bone histomorphometry

The femurs from 3-month-old male *Tmbim6* wild-type and knockout mice were isolated and fixed with a 4% paraformaldehyde solution, followed by decalcification in 0.5 M EDTA at pH 7.4. The femurs were then dehydrated with ethanol, cleared with xylene, and embedded in paraffin. The femur sections were cut to a thickness of 5 μm and stained with hematoxylin and eosin (H&E), tartrate-resistant acid phosphatase (TRAP), or alkaline phosphatase (ALP). For the histomorphometric analysis, we used the Osteomeasure software (Osteometrics, Atlanta, GA), following the nomenclature and abbreviations recommended by the Committee of the American Society for Bone and Mineral Research [39].

2.3. Osteoclast precursor cells isolation

Bone marrow cells were collected from femurs and tibias of 6–8-week-old C57BL/6 mice and cultured in minimum essential medium-α (MEM-α) supplemented with 10% FBS and M-CSF (5 ng/ml) for 16 h. Nonadherent cells were harvested and further cultured with M-CSF (30 ng/ml) for 3 days. After removal of floating cells, adherent cells were used as OCP cells [40].

2.4. Osteoclast differentiation and TRAP staining

OCP cells were cultured in the presence of M-CSF (30 ng/ml) and RANKL (100 ng/mL). After 3–6 days, cells were fixed and stained for tartrate-resistant acid phosphatase (TRAP) using an acid phosphatase leukocyte kit (Sigma, 386A). TRAP-positive multinucleated cells containing three or more nuclei were counted as osteoclasts under a light microscope [41].

2.5. Lentivirus-mediated shRNA transduction

DNA oligonucleotides encoding shRNAs specific for *Tmbim6* or non-target negative control were annealed and ligated into the lentiviral expression vector pLKO.1 (Addgene). Lentiviral particles were prepared as previously described [40,42]. To knockdown *Tmbim6*, OCP cells were infected with these viruses and selected with puromycin (2 μg/ml) for 2 days. OCP cells were then differentiated with M-CSF (30 ng/ml) and RANKL (100 ng/ml). The DNA oligonucleotides encoding the shRNAs are described in Supplementary Table 1.

2.6. Cell proliferation assay

OCP cells were cultured with M-CSF (30 ng/ml) and RANKL (100 ng/mL) on 96-well plates. Cell proliferation was evaluated using water soluble tetrazolium salt (WST) assay by measuring the absorbance at 450 nm (DoGen, Korea, EZ-3000).

2.7. Real-time quantitative PCR

Total RNA was prepared using Tri-RNA reagent (Favorgen, FATRR001) according to manufacturer's instruction, and cDNAs were generated from total RNAs via reverse transcription using M-MLV reverse transcriptase (Promega, M1708) according to the manufacturer's instructions. Real-time PCR was performed using IQ SYBR Green Supermix in an IQ5 real-time thermal cycler (Bio-Rad). Relative mRNA levels were normalized to β-actin mRNA levels. The primers used for PCR are described in Supplementary Table 2.

2.8. Intracellular reactive oxygen species (ROS) measurement

OCP cells were cultured in 96-well black/clear bottom plates with M-CSF (30 ng/mL) and RANKL (100 ng/mL) for 24 h. To detect intracellular ROS, the cells were preloaded with 5 μM of 2',7'-dichlorofluorescin diacetate (DCF-DA) in phenol red-free MEM-α for 1 h in the dark, and then treated with RANKL (100 ng/mL) for 30 min. The DCF fluorescence was measured on a fluorescence plate reader at excitation/emission wavelengths of 485/538 nm in endpoint mode [43–46]. Additionally, CellROXTM Deep Red Reagent (Molecular Probes) was used to detect intracellular ROS following the manufacturer's instructions. Briefly, cells were cultured and treated with or without RANKL for 10 min. CellROXTM Deep Red Reagent was added to a final concentration of 0.5 μM for 30 min before harvesting and detection. Signals were measured at 660 nm by flow cytometry (CytoFlex, Beckman Coulter), and the results are presented as the mean fluorescence intensity (MFI) of three independent experiments.

2.9. RNA-sequencing

For RNA-seq, OCP cells were seeded in the presence of M-CSF (30 ng/mL) onto 6-well culture plates treated with or without RANKL (100 ng/mL) for 24 h. After libraries were prepared from total RNA, high-throughput sequencing with 100 bp pair-end was performed from E-Biogen Inc. (Seoul, Korea) using HiSeq 2500 (Illumina, CA, USA). mRNA-Seq reads were aligned to reference mouse genome (mm10 assembly) using TopHat. HOMER program was used to analyze RNA-seq data performed as described [38,47]. The cut-off parameters were set at fold change $\geq$1.5 and FDR $<$0.05 (Benjamin-Hochberg). For K-means clustering and gene ontology (GO) analysis, we used the Morpheus web site (https://software.boradinstitute.org/morpheus/) and Metascape tool (https://metascape.org) [48]. To predict transcription factors associated with a set of genes, TRRUST V2 and ChEA3 tool were used [49,50]. RNA-seq data were available at NCBI Gene Expression Omnibus (GSE231889).

2.10. Preparation of whole-cell lysates and subcellular fractionation

For preparation of whole-cell lysates, cells were lysed in standard lysis buffer containing protease inhibitor, 1 mM sodium orthovanadate, and 2.5 mM sodium pyrophosphate. The cell lysates were subjected to SDS-PAGE, followed by immunoblotting with the indicated antibodies. To obtain the cytosolic and nuclear fractions, cells were resuspended in buffer A [10 mM HEPES (pH 7.9), 10 mM KCl, 1.5 mM $MgCl_2$, 0.34 M sucrose, 10% glycerol, 1 mM DTT, 0.1% Triton X-100, and protease inhibitors] and incubated on ice for 8 min. After centrifugation at 300$\times g$ for 5 min at 4 °C, the supernatant (cytosolic fraction) was collected in a new tube. The nuclear pellet was washed once with buffer A, lysed with SDS lysis buffer, and briefly sonicated (nuclear fraction). The nuclear fractions were followed by immunoblotting with the indicated antibodies. The antibodies used in the current study are listed in Supplementary Table 3.

2.11. Chromatin immunoprecipitation (ChIP) assay

Cells were crosslinked with 1% formaldehyde for 10 min and washed with ice-cold PBS. The crosslinked cells were lysed with hypotonic buffer [10 mM HEPES-KOH (pH 7.8), 10 mM KCl, 1.5 mM $MgCl_2$, and protease inhibitors] on ice for 10 min and centrifuged for 1 min at 14 000 rpm. The nuclear pellet was resuspended in nuclear lysis buffer [1% SDS, 50 mM Tris-HCl (pH 8.0), 10 mM EDTA, and protease inhibitors] for 1 h and sonicated using a Bioruptor (Diagenode) for 20 cycles. After preclearing, ChIP assays were performed using antibodies specific for p65 and control IgG [40,42,51,52]. The precipitated DNA was subjected to real-time quantitative PCR with primers specific for *Mmp-9* promoter region and *Tnfrsf11a* promoter region. The antibody and primers in this assay are listed in Supplementary Table 2 and Supplementary Table 3.

2.12. Measurement of total glutathione levels and GSH/GSSG ratios

To measure total glutathione levels and GSH/GSSG ratios, cells were seeded on 96-well plates with clear bottoms and white tops and treated with or without RANKL for 24 h. The GSH/GSSG-GloTM Assay kit (Promega) was used according to the manufacturer's instructions to measure total glutathione and oxidized glutathione (GSSG) levels. The total glutathione concentration was normalized to the protein concentration.

2.13. Statistical analysis

Data are presented as the mean ± SEM or the mean ± SD values. The exact numbers of replicates (n) are indicated in the figure legends. The significance of differences was evaluated using the two-tailed *t*-test or two-way ANOVA followed by Tukey's multiple comparison test for comparisons among three or more groups. A P value $<$ 0.05 was considered significant. In the figures, the asterisks denote statistical significance (*P $<$ 0.05; **P $<$ 0.01; ***P $<$ 0.001; ****P $<$ 0.000 1). Statistical analysis was performed in GraphPad Prism 9.

3. Results

3.1. TMBIM6 loss leads to osteoporosis by increasing osteoclast differentiation

To investigate the role of TMBIM6 in bone metabolism, the bone architecture of *Tmbim6* knockout male mice was analyzed by micro-CT analysis. In *Tmbim6* knockout mice, bone mass was significantly reduced compared to that in littermate *Tmbim6* wild-type mice (Fig. 1A). As expected, bone mineral density, trabecular thickness (Tb.Th), trabecular number (Tb.N), and trabecular volume (Tb.V) in *Tmbim6* knockout mice were decreased compared to those in *Tmbim6* wild-type littermates, but trabecular space (Tb.sp) was increased (Fig. 1B). To further understand the effects of Tmbim6 on bone metabolism, femurs from *Tmbim6* wild-type and knockout mice were analyzed by TRAP staining. The number of TRAP-positive osteoclasts was higher in TMBIM6 knockout mice than in *Tmbim6* wild-type mice (Fig. 1C). Histomorphometric analysis further revealed that trabecular osteoclast numbers (N.Oc/B.Pm), osteoclast surface area (Oc.S/BS), as well as bone resorption activity (ES/BS) were higher in *Tmbim*6 knockout mice. Conversely, the number of ALP-positive cells, osteoblast surface area (Ob.S/BC) and trabecular bone volume versus tissue volume (BV/TV) were higher in *Tmbim6* wild-type mice than in TMBIM6 knockout mice (Fig. 1C and D; Fig. S1). These results suggest that *Tmbim6* loss resulted in an osteoporotic phenotype characterized by increased osteoclast activity and decreased bone formation.

3.2. TMBIM6 inhibits RANKL-induced osteclastogenesis

To investigate the role of TMBIM6 on osteclastogenesis and osteoblastogenesis. We first performed TRAP staining using OCP cells from *Tmbim6* knockout and *Tmbim6* wild-type mice. TMBIM6 knockout resulted in a significant increase in osteoclast formation, characterized by a higher number of nuclei per cell. (Fig. 2A and Fig. S2A). Similar results were observed in *Tmbim6* knockdown cells (Fig. 2B and Fig. S2B). Notably, the finding that *Tmbim6* knockdown had little effect on OCP proliferation suggested that TMBIM6 selectively inhibited the differentiation, but not the proliferation of, OCP cells (Fig. 2C). We also examined whether TMBIM6 could regulate the expression of osteoclast marker genes such as NFATc1. Our results showed that knockout or knockdown of *Tmbim6* led to a significant increase in the expression of osteoclast-related genes after RANKL treatment (Fig. 2D and Fig. S2C). These findings suggest that TMBIM6 acts as a suppressor of RANKL-induced osteoclast formation. Given that TMBIM6 inhibits ROS production [34,53,54], and RANKL induces ROS in OCP cells [17,18,55], we hypothesized that TMBIM6 may suppress RANKL-mediated ROS generation, thereby suppressing osteoclast formation. Indeed, we found that ROS levels were substantially increased in TMBIM6-depleted OCP cells compared to those in TMBIM6 wild-type cells after RANKL treatment (Fig. 2E and F). Furthermore, we investigated the role of TMBIM6 in osteoblast differentiation by depleting it in both primary calvarial osteoblasts and a preosteoblastic cell line, MC3T3-E1. Our results showed that TMBIM6 knockdown hindered osteoblast differentiation, as revealed by ALP staining, and significantly impeded cell proliferation (Figs. S2D and S2E). These results suggest that TMBIM6's antiapoptotic function is crucial for osteoblast differentiation. Although TMBIM6 is involved in both osteoclasts and osteoblasts, we specifically focused on investigating its role in osteoclast differentiation. This decision was based on the observation that TMBIM6 predominantly influences osteoclast differentiation rather than proliferation, which differs from its effects on osteoblast.

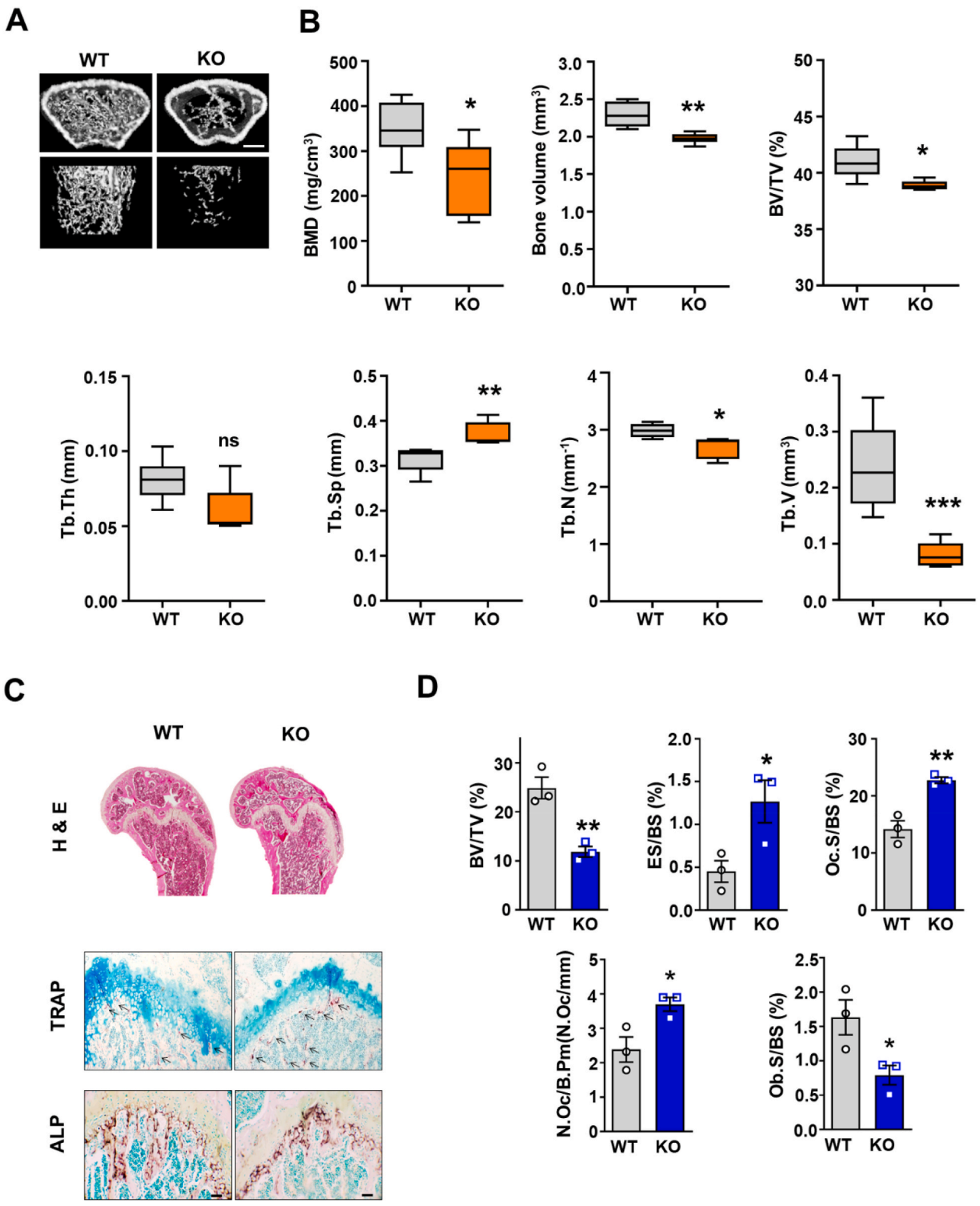

Fig. 1. TMBIM6-depleted mice exhibit an osteoporotic phenotype.
A Representative micro-CT image of the proximal femur of 3-month-old male *Tmbim6* wild-type and knockout mice (top, axial view; bottom, longitudinal view). Scale bar, 1 mm. **B** Micro-CT analysis data of the femurs of 3-month-old male *Tmbim6* wild-type and knockout mice (n = 6). Box plots represent median with minimum and maximum whiskers. BMD, bone mineral density; BV/TV, trabecular bone volume per tissue volume; Tb.Th, trabecular thickness; Tb. Sp, trabecular spacing; Tb.N, trabecular number; Tb.V, trabecular volume. **C** H&E and TRAP staining of femur sections from 3-month-old male *Tmbim6* wild-type and knockout mice. The black arrows indicate TRAP-positive osteoclasts. Scale bar, 100 μm. **D** Histological analysis of femur sections from **C**. BV/TV, bone volume per tissue volume; ES/BS, eroded surface per bone surface; Oc. S/BS, osteoclast surface per bone surface; N. Oc/B.Pm, osteoclast number per bone perimeter; Ob. S/BS, osteoblast surface per bone surface. The data are presented as the mean ± SEM values. *P* value is determined by two-tailed *t*-test. $^{*}P < 0.05$; $^{**}P < 0.01$; $^{***}P < 0.001$; ns, not significant. WT, *Tmbim6* wild-type mice; KO, *Tmbim6* knockout mice.

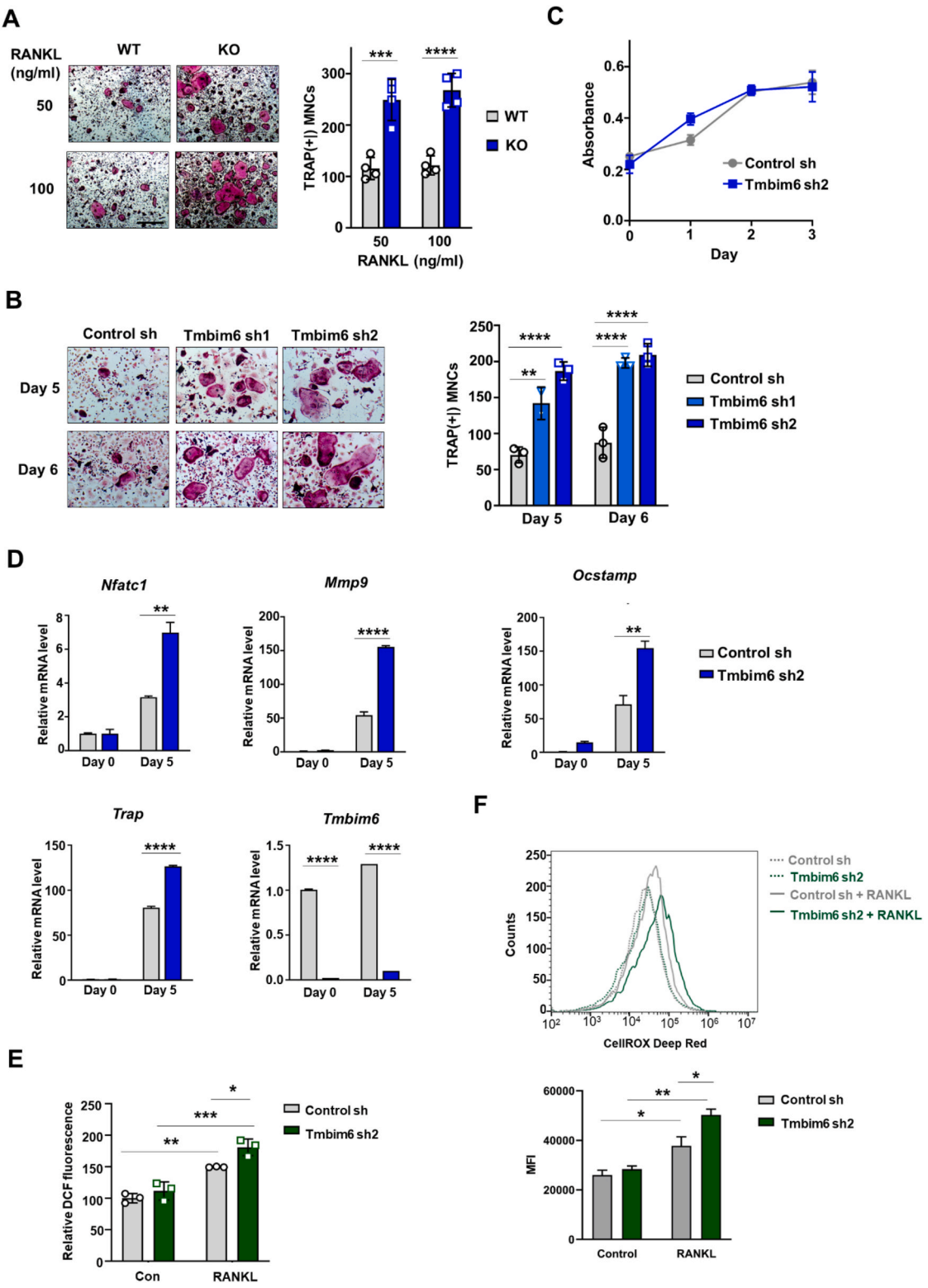

Fig. 2. TMBIM6 depletion augments RANKL-induced OC differentiation

A TRAP staining of osteoclasts precursors (OCP) cells from *Tmbim6* wild-type and knockout mice. Scale bar, 75 μm. **B** TRAP staining of OCP cells expressing control shRNA and *Tmbim6* shRNA. **C** Cell proliferation assay of mock- or TMBIM6-depleted OCP cells. **D** mRNA expression of *Nfatc1* and its target genes from mock- or TMBIM6-depleted OCP cells, as in **B**. **E** Levels of reactive oxygen species (ROS) of mock- or TMBIM6-depleted OCP cells were evaluated with DCF-DA in the absence or presence of RANKL (100 ng/ml, 30 min). F Flow cytometry histograms of cellular ROS measured by CellROX deep red. Bar graphs represent the median fluorescence intensity (MFI) of OCP cells in the absence or presence of RANKL (100 ng/ml, 10 min). The data are presented as the mean ± SD values of three independent experiments. *P* value is determined by two-way ANOVA. $^{*}P < 0.05$; $^{**}P < 0.01$; $^{***}P < 0.001$; $^{****}P < 0.0001$. (For interpretation of the references to colour in this figure legend, the reader is referred to the Web version of this article.)

3.3. TMBIM6 regulates the expression of a set of osteoclastogenic genes during osteoclastogenesis

We next examined whether TMBIM6 plays a role in the transcriptional regulation of genes associated with ROS response and osteoclast formation. To do this, we performed RNA-sequencing using mRNA from mock-depleted or TMBIM6-depleted OCP cells with or without RANKL treatment for 24 h. Genome-wide transcriptome analysis revealed that 3,364 genes were differentially expressed in pairwise comparisons among the four conditions. K-means clustering showed five gene clusters that were differentially affected by RANKL treatment and TMBIM6 depletion (Fig. 3A, Supplementary Table 4 and Supplementary Table 5). To determine gene function within each cluster, gene ontology (GO) terms were further analyzed (Fig. 3B). Interestingly, genes (cluster I) involved in the tumor necrosis factor signaling pathway, osteoclast differentiation, and NIK/NF-κB signaling were upregulated by RANKL treatment and further upregulated by TMBIM6 depletion (Fig. 3C). However, cluster V genes implicated in the response to ROS were downregulated by RANKL and further downregulated by TMBIM6 depletion (Fig. 3D). The GO analysis results were confirmed by qRT-PCR analysis (Fig. 3E).

3.4. TMBIM6 suppresses NF-κB-mediated osteoclastogenesis

Given that TMBIM6 negatively regulates the expression of osteoclast-related genes, resulting in the inhibition of RANKL-mediated osteoclast formation, we sought to find transcription factors that control the expression of genes affected by TMBIM6 during osteoclastogenesis. To do this, we analyzed 518 genes in cluster I using the TRRUST v2 and ChEA3 databases and found that canonical and non-canonical NF-κB transcription factors, such as RELA–NF-κB1 and RELB–NF-κB2, are commonly high-ranked (Fig. 4A and Fig. S3A). We then investigated the effect of TMBIM6 on the NF-κB signaling pathway. OCP cells expressing control shRNA or TMBIM6 shRNA were stimulated with RANKL for the indicated times (Fig. 4B), and the nuclear localization of NF-κB transcription factors was analyzed by western blotting. Interestingly, *Tmbim6* knockdown significantly enhanced the RANKL-induced nuclear translocation of RELA–NF-κB1, while it did not change the expression levels of RELA (Fig. 4B and Fig. S3B). Concomitantly, IκB degradation and p65 phosphorylation increased in TMBIM6-depleted OCP cells (Fig. 4C). In contrast, TMBIM6 had less effect on the RANKL-induced phosphorylation of ERK, p38, and JNK (Fig. 4C). To determine whether p65 is the primary target in the TMBIM6-mediated suppression of RANKL-induced osteoclastogenesis, we employed JSH-23 (an inhibitor of p65 nuclear translocation). As shown in Fig. 4D, JSH-23 completely stopped the increase in osteoclast formation induced by TMBIM6 knockdown. The results of the analysis for finding transcription factors (Fig. 4A and Fig. S3A) and previous chromatin immunoprecipitation (ChIP)-sequencing data [52] demonstrated that the p65 peaks were primarily enriched in the promoter regions of *Mmp-9, Nfatc1,* and *Tnfrsf11a* genes (Fig. S3C). Furthermore, JSH-23 treatment significantly repressed mRNA expressions of *Mmp-9*, *Nfatc1*, and *Tnfrsf11a* (Fig. S3D). These results strongly suggested that TMBIM6 controls the expression of osteoclast-specific genes induced by RANKL mainly through the NF-κB signaling pathway. To reinforce these findings, we examined whether p65 is localized at the promoters of the *Mmp-9* and *Tnfrsf11a* in response to RANKL treatment. We next analyzed the effect of TMBIM6 on p65 localization. Control OCP cells and OCP cells depleted of TMBIM6 were treated with RANKL for 30 min. ChIP assays using p65 antibody demonstrated that TMBIM6 depletion severely increased p65 localization at the *Mmp-9* and *Tnfrsf11a* promoters (Fig. 5A). *Tmbim6* knockdown significantly induced *Mmp-9* and *Tnfrsf11a* expression (Fig. 5B). These findings indicate that TMBIM6 functions as a negative regulator of NF-κB-mediated osteoclastogenesis.

3.5. Redox regulation of antioxidant inhibits NF-κB activation induced by TMBIM6 depletion

Recent studies have demonstrated that ROS induces NF-κB nuclear translocation [56–59]. Given our findings that TMBIM6 depletion increases ROS production (Fig. 2E and F) and NF-κB nuclear translocation (Fig. 4B), we hypothesized that N-acetyl cysteine (NAC) could eliminate ROS induced by TMBIM6 depletion and thereby abrogate NF-κB activity. We first determined the optimal concentration of NAC to inhibit osteoclast differentiation but not proliferation. NAC (2.5 mM, 5 mM and 10 mM) selectively inhibited osteoclast differentiation (Fig. 6A and Fig. S4A). We next investigated whether NAC modulates TMBIM6-dependent OC formation. As expected, TMBIM6 depletion increased RANKL-mediated osteoclast formation compared to that in control shRNA-treated osteoclasts; NAC treatment abrogated this effect of TMBIM6 depletion on osteoclastogenesis (Fig. 6B). Consistent with these results, the ROS level increase in TMBIM6-depleted cells was reduced by NAC treatment (Fig. 6C). Furthermore, nuclear translocation of NF-κB increased by TMBIM6 depletion was decreased to the level achieved by control shRNA (Fig. 6D and Fig. S4B). As expected, ChIP and qRT-PCR experiments using OCP cells depleted of TMBIM6 clearly showed that NAC treatment significantly reduced the localization of p65 at *Mmp9* and *Tnfrsf11a* promoters, leading to the inhibition of target gene transcription (Fig. 6E and F). Taken together, these data support our hypothesis that TMBIM6-mediated redox regulation is critical in fine-tuning the localization and function of p65 during osteoclastogenesis.

3.6. TMBIM6 controls redox regulation via NRF2 signaling pathways

Previous studies have established that TMBIM6 has the capacity to activate NRF2, a critical transcription factor that plays a crucial role in regulating the cellular antioxidant response [54,60]. To investigate the potential role of TMBIM6 in redox regulation via the NRF2 signaling pathway, we conducted a comprehensive analysis of the expression levels of NRF2 in TMBIM6-depleted cells. Our Western blotting and qRT-PCR analyses clearly indicated that TMBIM6 depletion resulted in a notable reduction in both the mRNA and protein levels of NRF2 (Figs. 3E and 7A). These findings suggest that TMBIM6 is involved in regulating the expression of NRF2. Additionally, we observed a significant decrease in the nuclear translocation of NRF2 in TMBIM6-depleted cells, indicating that TMBIM6 plays a crucial role in facilitating the proper translocation of NRF2 to the nucleus, where it acts as a transcription factor to regulate gene expression. Consistent with this, we found that the mRNA expression of major ROS scavenging enzymes, including *Prdx1*, *Cat* and *Gpx1*, and the protein expression of PRDX1, which are known target genes of NRF2, were decreased upon TMBIM6 depletion (Fig. 7A and B). Furthermore, we observed a decrease in the GSH/GSSG ratio without any significant changes in total glutathione levels upon TMBIM6 depletion, indicating that TMBIM6 modulates cellular antioxidant response and ROS levels through the activation of NRF2 and its target genes (Fig. 7C and D).

4. Discussion

Recent studies have investigated the pathophysiological functions of TMBIM6 in cancer development and obesity; however, its biological significance in bone development remains unclear. In this study, we demonstrated that TMBIM6 functions as a negative regulator of osteoclastogenesis by scavenging reactive oxygen species (ROS). Using knockout mice and an ex vivo model, we observed that *Tmbim6* knockout accelerated RANKL-induced osteoclast differentiation. We also found that depletion of TMBIM6 suppressed the proliferation of preosteoblasts, which in turn led to the inhibition of osteoblast differentiation. Several studies have shown that ROS can prevent osteoblast differentiation by inducing apoptosis [61–63]. Our study, along with

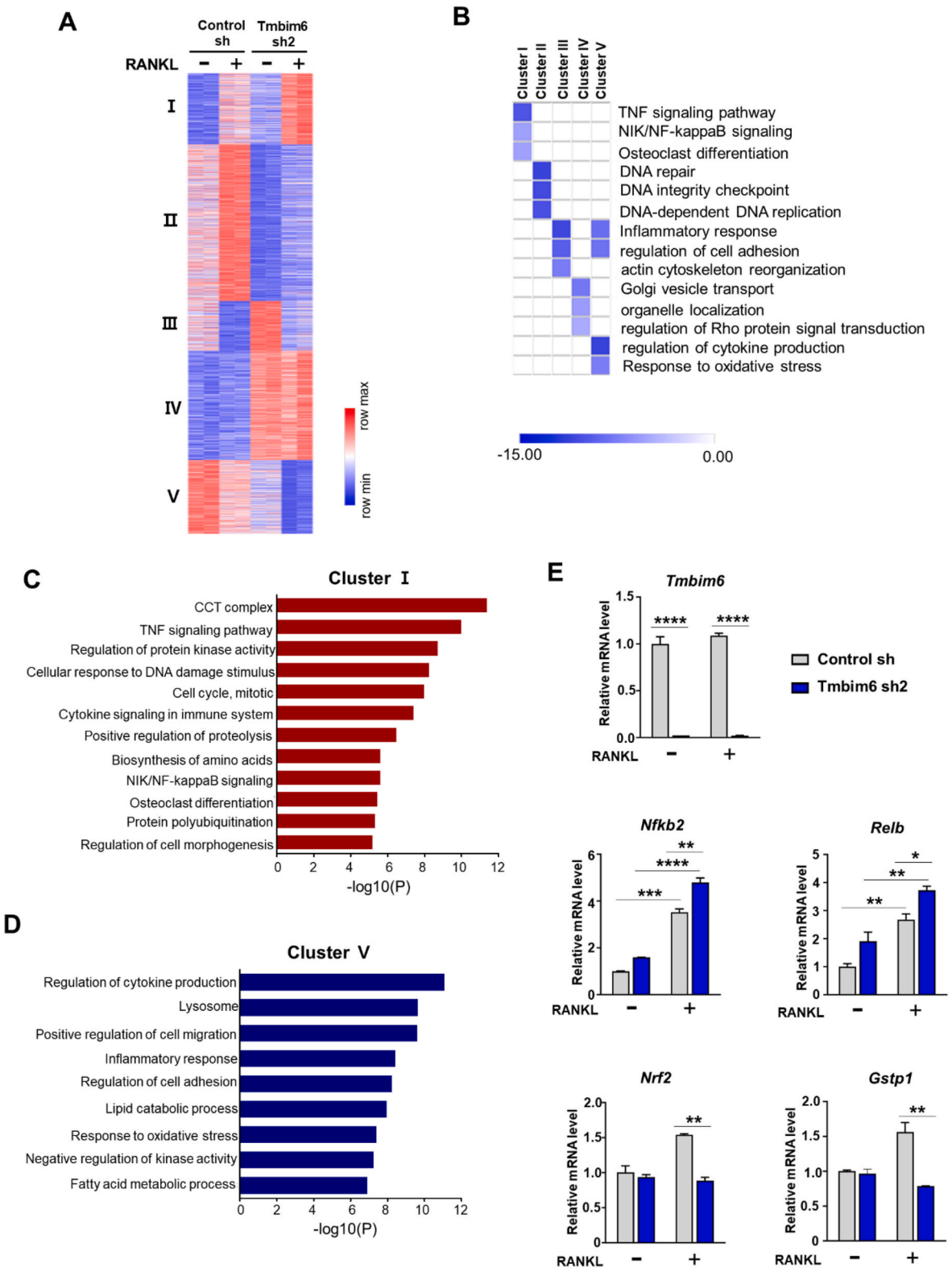

Fig. 3. *Tmbim6* knockdown alters the gene expression profile in RANKL-induced osteoclast differentiation

A K-means (K = 5) clustering of 3,364 differentially expressed genes in any pairwise comparison among four conditions. Mock-depleted and TMBIM6-depleted OCP cells were treated with or without RANKL (100 ng/ml) for 24 h. RNA sequencing were performed using total mRNA. **B** Heatmap showing the *p*-value-based significance of gene ontology (GO) term enrichment for genes in each cluster. **C** GO analysis of Cluster I. **D** GO analysis of Cluster V. **E** qRT-PCR analysis of the representative genes for clusters I and V in mock- and TMBIM6-depleted OCP cells treated with or without RANKL (100 ng/ml) for 24 h. The data are presented as the mean ± SD values of three independent experiments. *P* value is determined by two-way ANOVA. $^{*}P < 0.05$; $^{**}P < 0.01$; $^{***}P < 0.001$; $^{****}P < 0.0001$.

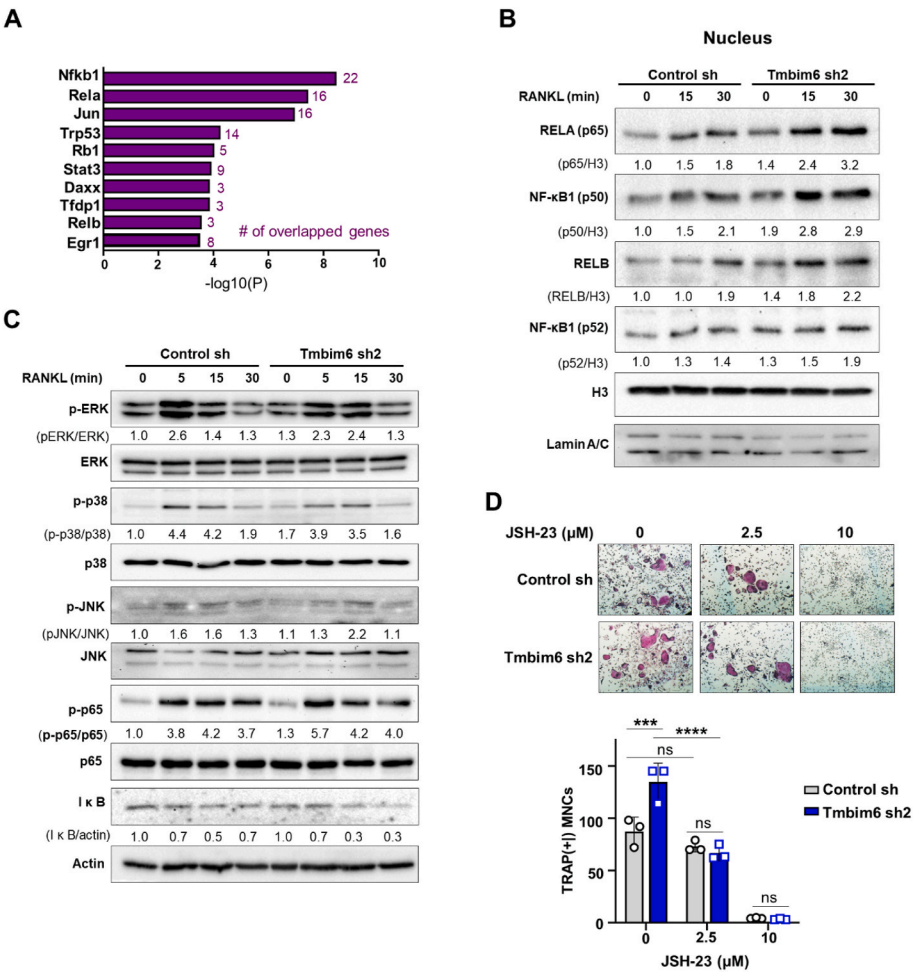

Fig. 4. TMBIM6 depletion enhances the NF-κB translocation induced by RANKL
A Prediction of transcription factors regulating the expression of genes belonging to cluster I, as in Fig. 3A, using TRRUST v2. **B** Effect of *Tmbim6* knockdown on NF-κB nuclear localization upon RANKL treatment. The western blot band was quantified using Image J software and shown as the relative ratio of each protein band intensity normalized to H3 band intensity. **C** Effect of *Tmbim6* knockdown on the NF-κB and MAPK signaling pathways upon RANKL treatment. The western blot band was quantified using Image J software and shown as the relative ratio of each protein band intensity normalized to total protein band or actin band intensity. **D** Effect of JSH-23 on osteoclast differentiation from OCP cells expressing control shRNA and *Tmbim6* shRNA2. The data are presented as the mean ± SD values of three independent experiments. P value is determined by two-way ANOVA. *P < 0.05; **P < 0.01; ***P < 0.001; ****P < 0.0001; ns, not significant.

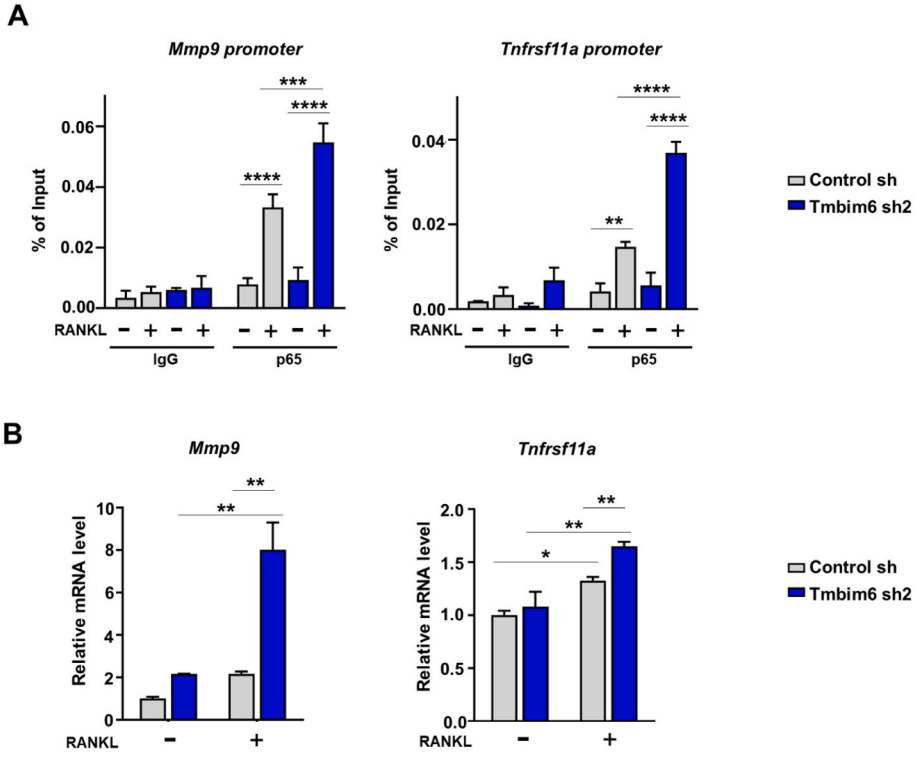

Fig. 5. Effect of *Tmbim6* knockdown on p65 localization to target genes. **A** ChIP assay of p65 localization at the *Mmp-9* (−0.5 kb) or *Tnfrsf11a* (−0.5 kb) promoter in TMBIM6-depleted cells upon RANKL signaling (100 ng/ml, 30 min). **B** mRNA expression of *Mmp-9* and *Tnfrsf11a* from mock- or TMBIM6-depleted cells with or without RANKL treatment for 24 h. The data are presented as the mean ± SD values of three independent experiments. P value is determined by two-way ANOVA. *P < 0.05; **P < 0.01; ***P < 0.001; ****P < 0.0001.

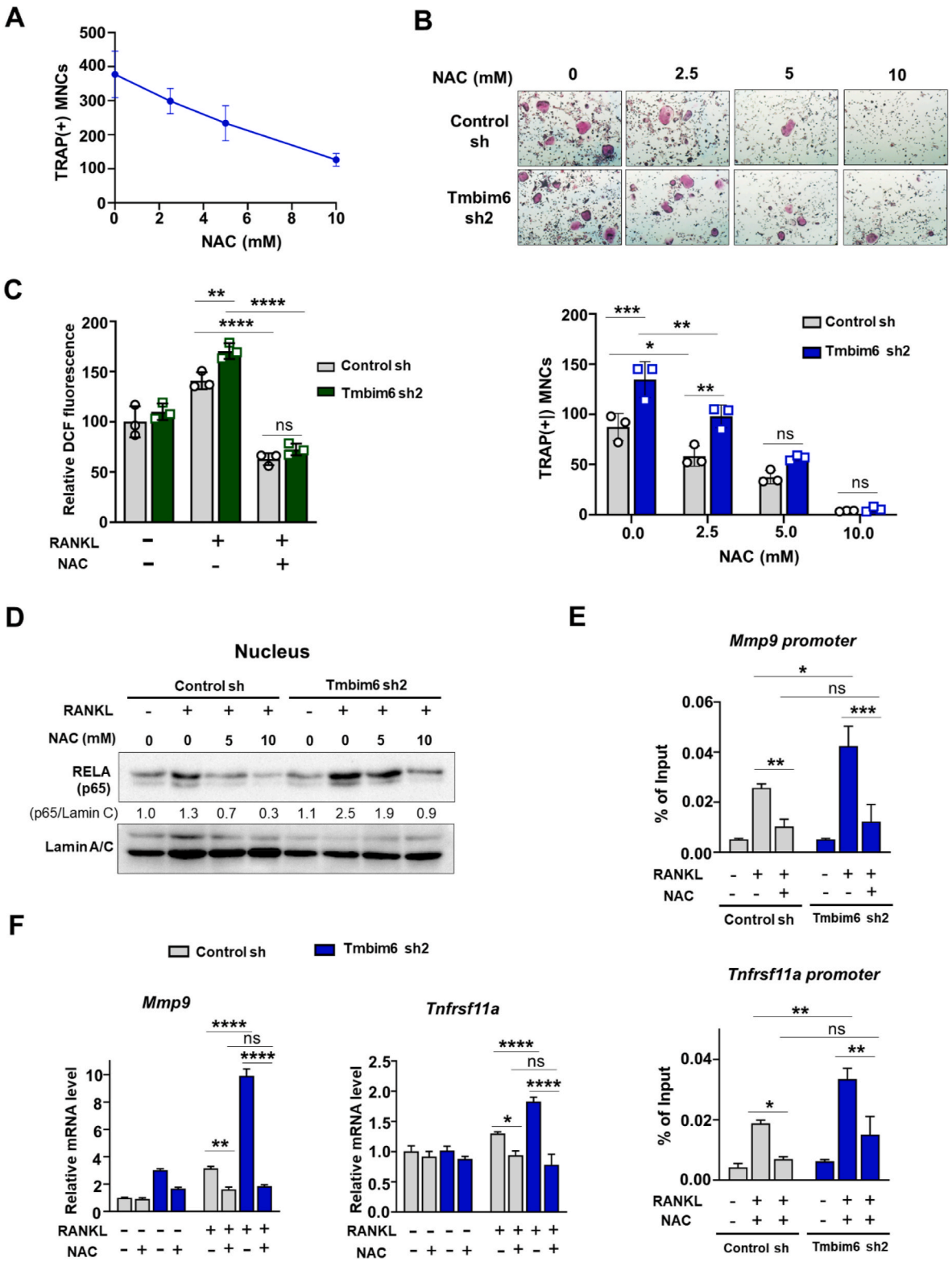

Fig. 6. Antioxidant NAC represses the NF-κB activation induced by TMBIM6 depletion.
A Determination of the optimal concentration of NAC to inhibit osteoclast differentiation. OCP cells treated with the indicated concentrations of NAC were stimulated with M-CSF (30 ng/ml) and RANKL (100 ng/mL) and TRAP staining was performed. **B**TRAP staining of OCP cells expressing control shRNA and *Tmbim6* shRNA2 in the absence or presence of NAC. **C**ROS levels of mock- or TMBIM6-depleted OCP cells treated with RANKL (100 ng/ml, 30 min) in the absence or presence of NAC (10 mM). **D** Effect of NAC on the nuclear localization of p65 in TMBIM6-depleted cells. The western blot band was quantified using Image J software and shown as the relative ratio of each protein band intensity normalized to lamin C band intensity. **E** ChIP assay of p65 localization at the *Mmp-9* (−0.5 kb) or *Tnfrsf11a* (−0.5 kb) promoter in TMBIM6-depleted OCP cells upon RANKL signaling (100 ng/ml, 30 min) in the absence or presence of NAC (10 mM). **F** mRNA expression of *Mmp-9* and *Tnfrsf11a* from mock- or TMBIM6-depleted OCP cells stimulated with RANKL for 24 h in the absence or presence of NAC (10 mM). The data are presented as the mean ± SD values of three independent experiments. P value is determined by two-way ANOVA. *P < 0.05; **P < 0.01; ***P < 0.001; ****P < 0.0001; ns, not significant.

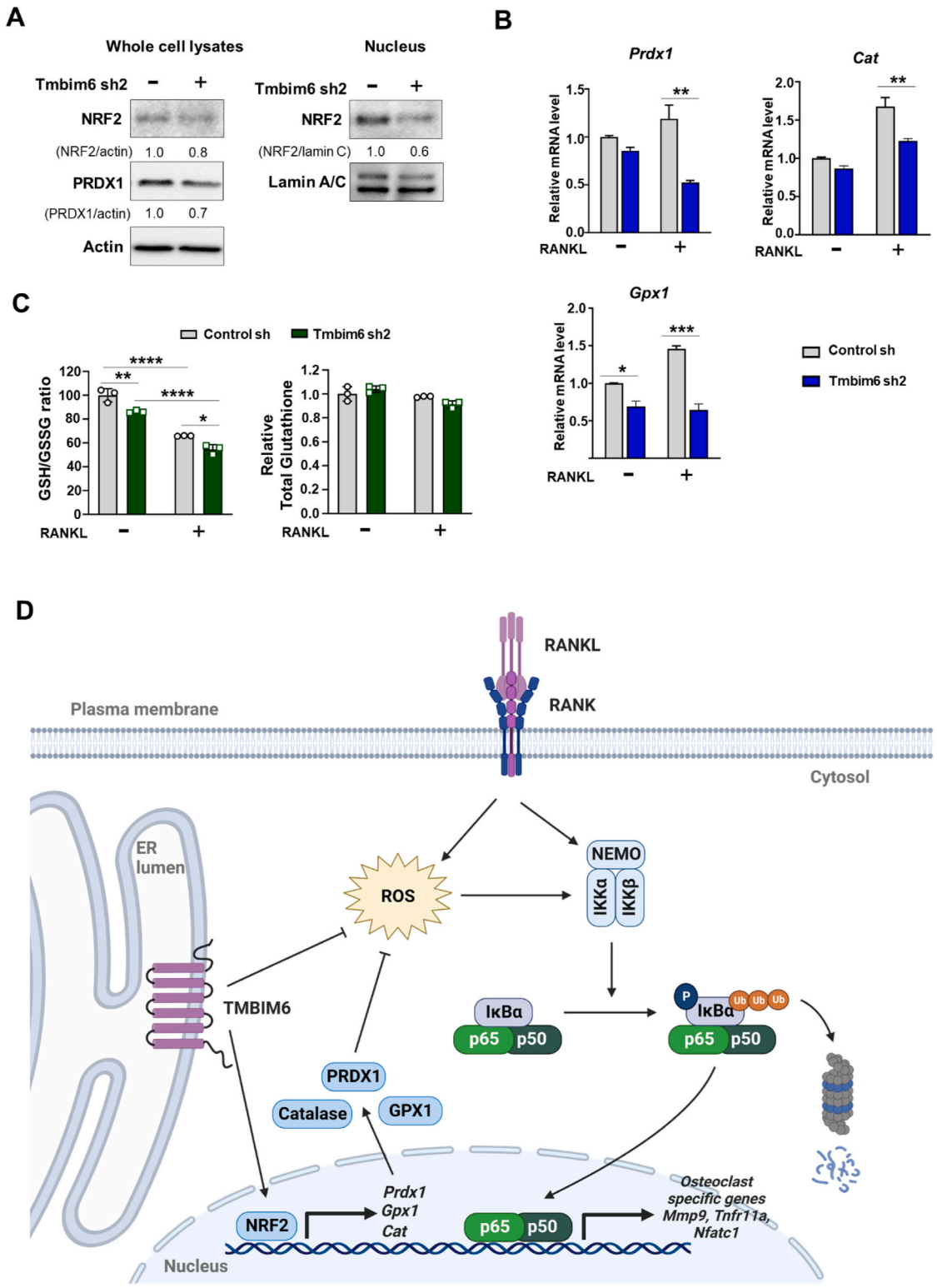

Fig. 7. TMBIM6 modulates cellular antioxidant response via regulating NRF2.
A Effect of *Tmbim6* knockdown on NRF2 protein expression and nuclear localization in the absence or presence of RANKL (100 ng/ml) for 24 h. The western blot band was quantified using Image J software and shown as the relative ratio of each protein band intensity normalized to actin or lamin C band intensity. **B** mRNA expression of ROS scavenging enzymes in mock- and TMBIM6-depleted OCP cells treated with or without RANKL (100 ng/ml) for 24 h. **C** Effect of *Tmbim6* knockdown on GSH/GSSG ratio and total glutathione level in the absence or presence of RANKL (100 ng/ml) for 24 h. **D** Schematic model demonstrating the putative role of TMBIM6 in RANKL-induced osteoclast differentiation. The binding of RANKL to RANK (TNFRSF11A) stimulates the NF-κB pathway via ROS generation leading to osteoclast differentiation. TMBIM6 inhibits ROS accumulation by inactivating ROS generator (e.g., cytochrome P450 (CYP)-NADPH-P450 reductase (NPR) complex) and/or activating ROS scavenger (e.g., PRDX1, catalase, and GPX1) through NRF2. Decreased ROS levels by TMBIM6 signaling pathways suppress RANKL-mediated p65 nuclear translocation, resulting in the inhibition of osteoclast differentiation.

others, has shown that TMBIM6 reduces ROS levels (as shown in Fig. 2E) [34,53,54], indicating that the antiapoptotic function of TMBIM6 is crucial for osteoblast differentiation. In summary, our study sheds light on the previously unknown role of TMBIM6 in bone development, highlighting its function as a negative regulator of osteoclastogenesis and a positive regulator of osteoblast differentiation through redox regulation.

Osteoblasts are known to regulate osteoclast differentiation by secreting M-CSF, RANKL, and OPG [2]. While the present study has demonstrated the cell-intrinsic role of TMBIM6 in both osteoblast and osteoclast development, the use of conventional knockout mice leaves it unclear whether the ablation of TMBIM6 in osteoblasts directly affects osteoclasts. To address this issue, a conditional knockout mouse model with TMBIM6 removed only from osteoblasts would be necessary.

Our GO and transcription factor finding analyses implied that TMBIM6 modulates the NF-κB signaling pathway. We found that the p65 nuclear translocation was increased when TMBIM6 was depleted. Concomitantly, we observed that TMBIM6 depletion rapidly degraded IκB without affecting MAPK signaling pathways. Recent studies have shown that ROS facilitated IKK-mediated IκB degradation [56–58]. Several studies have revealed that TMBIM6 inhibited ROS by disrupting the cytochrome P450 (CYP)-NADPH-P450 reductase (NPR) complex and/or activating nuclear factor erythroid 2-related factor 2 (NRF2) that controls the expression of antioxidant enzymes such heme oxygenase-1 and peroxiredoxin 1 (PRDX1) [26,53,54,64–67]. These results suggest that TMBIM6 inhibits IKK/NF-κB signaling pathways by reducing ROS generation. Indeed, *Tmbim6* knockdown suppressed the expression of various genes related to ROS scavenging (e.g., *Prdx1, Gpx1* and *Cat*). Our unpublished data revealed that *Prdx1* deletion in osteoclasts accelerates osteoclast differentiation. Consistent with this result, *Prdx1* knockout mice displayed decreased bone mass (data not shown). Moreover, NAC treatment reduced p65 nuclear translocation and inhibited osteoclast differentiation by abrogating the oxidative stress induced by TMBIM6 deficiency. These findings indicate that TMBIM6 acts as a redox regulator that modulates osteoclast differentiation.

The major sources of cellular ROS are NADPH oxidases and mitochondria. Srinivasan et al. have provided significant insights into the involvement of mitochondrial ROS in osteoclastogenesis and bone resorption [68,69]. They suggested that mitochondrial ROS act as signaling molecules that are crucial for osteoclast differentiation and bone resorption by regulating the expression of key osteoclast genes, including RANK, NFATc1, and TRAP. Similarly, another group [17,68] has demonstrated that ROS generated by NOX in osteoclasts play a crucial role in osteoclast differentiation. Although the exact mechanism by which RANKL regulates ROS production is not fully understood, it may involve the modulation of mitochondrial function, NADPH oxidase activity, or other ROS-generating enzymes. TMBIM6 is present in both the mitochondria and endoplasmic reticulum, where it regulates calcium signaling and mitochondrial function. In this study, we found that TMBIM6 plays a critical role in scavenging intracellular ROS during osteoclastogenesis by regulating NRF2-mediated antioxidant enzymes, including PRDX1. It is worth exploring whether TMBIM6 also regulates mitochondrial ROS levels, given that several mitochondrial antioxidant enzymes, such as SOD2, PRDX3, and PRDX5, are downstream targets of NRF2. Further studies are required to fully elucidate the precise molecular mechanisms underlying TMBIM6-mediated regulation of ROS levels in mitochondria.

Based on our findings from the present and previous studies, we propose a working model demonstrating how TMBIM6 regulates RANKL-induced osteoclast differentiation (Fig. 7D). The RANKL-RANK signaling pathway generates ROS, which activates NF-κB signaling pathways leading to the nuclear translocation of p65 and its localization to target gene promoters. In contrast, TMBIM6 promotes the nuclear translocation and transcription of NRF2 in response to oxidative stress, thereby enhancing antioxidant gene expression. Antioxidant enzymes, such as PRDX1, catalase, and GPX1, may antagonize NF-κB signaling by reducing ROS levels. Further studies are required to determine how RANKL-mediated oxidative stress overcomes TMBIM6-NRF2-antioxidant signaling pathways.

Declaration of competing interest

The authors declare that they have no known competing financial interests or personal relationships that could have appeared to influence the work reported in this paper.

Data availability

Data will be made available on request.

Acknowledgements

This work was carried out with the support of the National Research Foundation of Korea (2020R1A6A1A06046235, 2021RIS-001 and 2023R1A2C1006401 to K.K.; 2022R1I1A1A01069534 to S.J.Y.) and the Bio & Medical Technology Development Program (NRF-2017M3A9E4047243 to H.R.K.)

Appendix A. Supplementary data

Supplementary data to this article can be found online at https://doi.org/10.1016/j.redox.2023.102804.

References

[1] R. Florencio-Silva, et al., Biology of bone tissue: structure, function, and factors that influence bone cells, BioMed Res. Int. 2015 (2015), 421746, https://doi.org/10.1155/2015/421746.
[2] X. Feng, J.M. McDonald, Disorders of bone remodeling, Annu. Rev. Pathol. 6 (2011) 121–145, https://doi.org/10.1146/annurev-pathol-011110-130203.
[3] C. Sobacchi, et al., Osteopetrosis: genetics, treatment and new insights into osteoclast function, Nat. Rev. Endocrinol. 9 (2013) 522–536, https://doi.org/10.1038/nrendo.2013.137.
[4] W.J. Boyle, et al., Osteoclast differentiation and activation, Nature 423 (2003) 337–342, https://doi.org/10.1038/nature01658.
[5] K.H. Park-Min, Epigenetic regulation of bone cells, Connect. Tissue Res. 58 (2017) 76–89, https://doi.org/10.1080/03008207.2016.1177037.
[6] Y. Han, et al., Paracrine and endocrine actions of bone-the functions of secretory proteins from osteoblasts, osteocytes, and osteoclasts, BONE RES 6 (2018) 16, https://doi.org/10.1038/s41413-018-0019-6.
[7] S. Tanaka, et al., Macrophage colony-stimulating factor is indispensable for both proliferation and differentiation of osteoclast progenitors, J. Clin. Invest. 91 (1993) 257–263, https://doi.org/10.1172/JCI116179.
[8] B.F. Boyce, et al., NF-kappaB-Mediated regulation of osteoclastogenesis, Endocrinol. Metab. (Seoul) 30 (2015) 35–44, https://doi.org/10.3803/EnM.2015.30.1.35.
[9] S. Vaira, et al., RelA/p65 promotes osteoclast differentiation by blocking a RANKL-induced apoptotic JNK pathway in mice, J. Clin. Invest. 118 (2008) 2088–2097, https://doi.org/10.1172/JCI33392.
[10] K. Lee, et al., Roles of mitogen-activated protein kinases in osteoclast biology, Int. J. Mol. Sci. 19 (2018), https://doi.org/10.3390/ijms19103004.
[11] E.F. Wagner, R. Eferl, Fos/AP-1 proteins in bone and the immune system, Immunol. Rev. 208 (2005) 126–140, https://doi.org/10.1111/j.0105-2896.2005.00332.x.
[12] H. Takayanagi, et al., Induction and activation of the transcription factor NFATc1 (NFAT2) integrate RANKL signaling in terminal differentiation of osteoclasts, Dev. Cell 3 (2002) 889–901, https://doi.org/10.1016/s1534-5807(02)00369-6.
[13] J.H. Kim, N. Kim, Regulation of NFATc1 in osteoclast differentiation, J. Bone Metab. 21 (2014) 233–241, https://doi.org/10.11005/jbm.2014.21.4.233.
[14] S.J. Yi, et al., Bone remodeling: histone modifications as fate determinants of bone cell differentiation, Int. J. Mol. Sci. 20 (2019), https://doi.org/10.3390/ijms20133147.
[15] H. Kim, et al., SOD2 and Sirt3 control osteoclastogenesis by regulating mitochondrial ROS, J. Bone Miner. Res. 32 (2017) 397–406, https://doi.org/10.1002/jbmr.2974.
[16] S. Hyeon, et al., Nrf2 deficiency induces oxidative stress and promotes RANKL-induced osteoclast differentiation, Free Radic. Biol. Med. 65 (2013) 789–799, https://doi.org/10.1016/j.freeradbiomed.2013.08.005.
[17] N.K. Lee, et al., A crucial role for reactive oxygen species in RANKL-induced osteoclast differentiation, Blood 106 (2005) 852–859, https://doi.org/10.1182/blood-2004-09-3662.
[18] M.S. Kim, et al., RANKL-mediated reactive oxygen species pathway that induces long lasting Ca2+ oscillations essential for osteoclastogenesis, J. Biol. Chem. 285 (2010) 6913–6921, https://doi.org/10.1074/jbc.M109.051557.

[19] S.M. Bartell, et al., FoxO proteins restrain osteoclastogenesis and bone resorption by attenuating H2O2 accumulation, Nat. Commun. 5 (2014) 3773, https://doi.org/10.1038/ncomms4773.

[20] D.A. Callaway, J.X. Jiang, Reactive oxygen species and oxidative stress in osteoclastogenesis, skeletal aging and bone diseases, J. Bone Miner. Metabol. 33 (2015) 359–370, https://doi.org/10.1007/s00774-015-0656-4.

[21] D. Rojas-Rivera, C. Hetz, TMBIM protein family: ancestral regulators of cell death, Oncogene 34 (2015) 269–280, https://doi.org/10.1038/onc.2014.6.

[22] Q. Xu, J.C. Reed, Bax inhibitor-1, a mammalian apoptosis suppressor identified by functional screening in yeast, Mol. Cell 1 (1998) 337–346, https://doi.org/10.1016/s1097-2765(00)80034-9.

[23] J.H. Kim, et al., Role of BI-1 (TEGT)-mediated ERK1/2 activation in mitochondria-mediated apoptosis and splenomegaly in BI-1 transgenic mice, Biochim. Biophys. Acta 1823 (2012) 876–888, https://doi.org/10.1016/j.bbamcr.2012.01.016.

[24] D. Doycheva, et al., Adenoviral TMBIM6 vector attenuates ER-stress-induced apoptosis in a neonatal hypoxic-ischemic rat model, Dis. Model Mech. 12 (2019), https://doi.org/10.1242/dmm.040352.

[25] H.J. Chae, et al., BI-1 regulates an apoptosis pathway linked to endoplasmic reticulum stress, Mol. Cell 15 (2004) 355–366, https://doi.org/10.1016/j.molcel.2004.06.038.

[26] C. Lebeaupin, et al., BAX inhibitor-1: between stress and survival, FEBS J. 287 (2020) 1722–1736, https://doi.org/10.1111/febs.15179.

[27] D. Lisak, et al., BAX inhibitor-1 is a Ca(2+) channel critically important for immune cell function and survival, Cell Death Differ. 23 (2016) 358–368, https://doi.org/10.1038/cdd.2015.115.

[28] K.S. Robinson, et al., Bax inhibitor 1 in apoptosis and disease, Oncogene 30 (2011) 2391–2400, https://doi.org/10.1038/onc.2010.636.

[29] H.K. Kim, et al., TMBIM6/BI-1 contributes to cancer progression through assembly with mTORC2 and AKT activation, Nat. Commun. 11 (2020) 4012, https://doi.org/10.1038/s41467-020-17802-4.

[30] H.K. Kim, et al., TMBIM6 (transmembrane BAX inhibitor motif containing 6) enhances autophagy through regulation of lysosomal calcium, Autophagy 17 (2021) 761–778, https://doi.org/10.1080/15548627.2020.1732161.

[31] B. Bailly-Maitre, et al., Mice lacking bi-1 gene show accelerated liver regeneration, Cancer Res. 67 (2007) 1442–1450, https://doi.org/10.1158/0008-5472.CAN-06-0850.

[32] K. Philippaert, et al., Bax inhibitor-1 deficiency leads to obesity by increasing Ca(2+)-dependent insulin secretion, J. Mol. Med. (Berl.) 98 (2020) 849–862, https://doi.org/10.1007/s00109-020-01914-x.

[33] G.H. Lee, et al., Effect of BI-1 on insulin resistance through regulation of CYP2E1, Sci. Rep. 6 (2016), 32229, https://doi.org/10.1038/srep32229.

[34] H.K. Kim, et al., Transmembrane BAX Inhibitor Motif-6 (TMBIM6) protects against cisplatin-induced testicular toxicity, Hum. Reprod. 33 (2018) 378–389, https://doi.org/10.1093/humrep/dex381.

[35] K.R. Bhattarai, et al., TMBIM6 regulates redox-associated posttranslational modifications of IRE1alpha and ER stress response failure in aging mice and humans, Redox Biol. 47 (2021), 102128, https://doi.org/10.1016/j.redox.2021.102128.

[36] Y.P. Aryal, et al., An endoplasmic reticulum stress regulator, Tmbim6, modulates secretory stage of mice molar, J. Cell. Physiol. 234 (2019) 20354–20365, https://doi.org/10.1002/jcp.28635.

[37] G.H. Lee, et al., An acidic pH environment increases cell death and pro-inflammatory cytokine release in osteoblasts: the involvement of BAX inhibitor-1, Int. J. Biochem. Cell Biol. 43 (2011) 1305–1317, https://doi.org/10.1016/j.biocel.2011.05.004.

[38] K. Lee, et al., Transcriptome analysis reveals that abeliophyllum distichum nakai extract inhibits RANKL-mediated osteoclastogenensis mainly through suppressing Nfatc1 expression, Biology 9 (2020), https://doi.org/10.3390/biology9080212.

[39] D.W. Dempster, et al., Standardized nomenclature, symbols, and units for bone histomorphometry: a 2012 update of the report of the ASBMR Histomorphometry Nomenclature Committee, J. Bone Miner. Res. 28 (2013) 2–17, https://doi.org/10.1002/jbmr.1805.

[40] D. An, et al., Defective entry into mitosis 1 (Dim1) negatively regulates osteoclastogenesis by inhibiting the expression of nuclear factor of activated T-cells, cytoplasmic, calcineurin-dependent 1 (NFATc1), J. Biol. Chem. 289 (2014) 24366–24373, https://doi.org/10.1074/jbc.M114.563817.

[41] Y. Kim, et al., Tetracycline analogs inhibit osteoclast differentiation by suppressing MMP-9-mediated histone H3 cleavage, Int. J. Mol. Sci. 20 (2019), https://doi.org/10.3390/ijms20164038.

[42] J. Kim, et al., Regulation of breast cancer-induced osteoclastogenesis by MacroH2A1.2 involving EZH2-mediated H3K27me3, Cell Rep. 24 (2018) 224–237, https://doi.org/10.1016/j.celrep.2018.06.020.

[43] I.J. Moon, et al., Ursodeoxycholic acid may inhibit environmental aging-associated hyperpigmentation, Antioxidants 10 (2021), https://doi.org/10.3390/antiox10020267.

[44] J. Zhou, et al., Steap4 plays a critical role in osteoclastogenesis in vitro by regulating cellular iron/reactive oxygen species (ROS) levels and cAMP response element-binding protein (CREB) activation, J. Biol. Chem. 288 (2013) 30064–30074, https://doi.org/10.1074/jbc.M113.478750.

[45] Y. Ohyama, et al., The polymethoxy flavonoid sudachitin suppresses inflammatory bone destruction by directly inhibiting osteoclastogenesis due to reduced ROS production and MAPK activation in osteoclast precursors, PLoS One 13 (2018), e0191192, https://doi.org/10.1371/journal.pone.0191192.

[46] H. Sasaki, et al., Receptor activator of nuclear factor-kappaB ligand-induced mouse osteoclast differentiation is associated with switching between NADPH oxidase homologues, Free Radic. Biol. Med. 47 (2009) 189–199, https://doi.org/10.1016/j.freeradbiomed.2009.04.025.

[47] H. Lee, et al., Ethyl acetate fraction of aqueous extract of lentinula edodes inhibits osteoclastogenesis by suppressing NFATc1 expression, Int. J. Mol. Sci. 21 (2020), https://doi.org/10.3390/ijms21041347.

[48] Y. Zhou, et al., Metascape provides a biologist-oriented resource for the analysis of systems-level datasets, Nat. Commun. 10 (2019) 1523, https://doi.org/10.1038/s41467-019-09234-6.

[49] H. Han, et al., TRRUST v2: an expanded reference database of human and mouse transcriptional regulatory interactions, Nucleic Acids Res. 46 (2018) D380–D386, https://doi.org/10.1093/nar/gkx1013.

[50] A.B. Keenan, et al., ChEA3: transcription factor enrichment analysis by orthogonal omics integration, Nucleic Acids Res. 47 (2019) W212–W224, https://doi.org/10.1093/nar/gkz446.

[51] K. Kim, et al., MMP-9 facilitates selective proteolysis of the histone H3 tail at genes necessary for proficient osteoclastogenesis, Genes Dev. 30 (2016) 208–219, https://doi.org/10.1101/gad.268714.115.

[52] S.J. Yi, et al., The KDM4B-CCAR1-MED1 axis is a critical regulator of osteoclast differentiation and bone homeostasis, BONE RES 9 (2021) 27, https://doi.org/10.1038/s41413-021-00145-1.

[53] H.R. Kim, et al., Bax inhibitor 1 regulates ER-stress-induced ROS accumulation through the regulation of cytochrome P450 2E1, J. Cell Sci. 122 (2009) 1126–1133, https://doi.org/10.1242/jcs.038430.

[54] G.H. Lee, et al., Bax inhibitor-1 regulates endoplasmic reticulum stress-associated reactive oxygen species and heme oxygenase-1 expression, J. Biol. Chem. 282 (2007) 21618–21628, https://doi.org/10.1074/jbc.M700053200.

[55] H. Ha, et al., Reactive oxygen species mediate RANK signaling in osteoclasts, Exp. Cell Res. 301 (2004) 119–127, https://doi.org/10.1016/j.yexcr.2004.07.035.

[56] H. Kamata, et al., Hydrogen peroxide activates IkappaB kinases through phosphorylation of serine residues in the activation loops, FEBS Lett. 519 (2002) 231–237, https://doi.org/10.1016/s0014-5793(02)02712-6.

[57] M.J. Morgan, Z.G. Liu, Crosstalk of reactive oxygen species and NF-kappaB signaling, Cell Res. 21 (2011) 103–115, https://doi.org/10.1038/cr.2010.178.

[58] S. Schoonbroodt, et al., Crucial role of the amino-terminal tyrosine residue 42 and the carboxyl-terminal PEST domain of I kappa B alpha in NF-kappa B activation by an oxidative stress, J. Immunol. 164 (2000) 4292–4300, https://doi.org/10.4049/jimmunol.164.8.4292.

[59] Y. Weng, et al., Trem2 mediated Syk-dependent ROS amplification is essential for osteoclastogenesis in periodontitis microenvironment, Redox Biol. 40 (2021), 101849, https://doi.org/10.1016/j.redox.2020.101849.

[60] D. Doycheva, et al., Viral-mediated gene delivery of TMBIM6 protects the neonatal brain via disruption of NPR-CYP complex coupled with upregulation of Nrf-2 post-HI, J. Neuroinflammation 16 (2019) 174, https://doi.org/10.1186/s12974-019-1559-4.

[61] H. Tao, et al., ROS signaling cascades: dual regulations for osteoclast and osteoblast, Acta Biochim. Biophys. Sin. 52 (2020) 1055–1062, https://doi.org/10.1093/abbs/gmaa098.

[62] H. Yao, et al., Upregulation of SIRT1 inhibits H2O2-induced osteoblast apoptosis via FoxO1/beta-catenin pathway, Mol. Med. Rep. 17 (2018) 6681–6690, https://doi.org/10.3892/mmr.2018.8657.

[63] D. Ran, et al., Reactive oxygen species control osteoblast apoptosis through SIRT1/PGC-1alpha/P53(lys382) signaling, mediating the onset of Cd-induced osteoporosis, J. Agric. Food Chem. (2023), https://doi.org/10.1021/acs.jafc.2c08505.

[64] Y.J. Kim, et al., Human prx1 gene is a target of Nrf2 and is up-regulated by hypoxia/reoxygenation: implication to tumor biology, Cancer Res. 67 (2007) 546–554, https://doi.org/10.1158/0008-5472.CAN-06-2401.

[65] T. Ishii, et al., Transcription factor Nrf2 coordinately regulates a group of oxidative stress-inducible genes in macrophages, J. Biol. Chem. 275 (2000) 16023–16029, https://doi.org/10.1074/jbc.275.21.16023.

[66] J.D. Hayes, A.T. Dinkova-Kostova, The Nrf2 regulatory network provides an interface between redox and intermediary metabolism, Trends Biochem. Sci. 39 (2014) 199–218, https://doi.org/10.1016/j.tibs.2014.02.002.

[67] D. Doycheva, et al., The characteristics of the ancient cell death suppressor, TMBIM6, and its related signaling pathways after endoplasmic reticulum stress, J. Neurosci. Res. 98 (2020) 77–86, https://doi.org/10.1002/jnr.24434.

[68] T.S. Agidigbi, C. Kim, Reactive oxygen species in osteoclast differentiation and possible pharmaceutical targets of ROS-mediated osteoclast diseases, Int. J. Mol. Sci. 20 (2019), https://doi.org/10.3390/ijms20143576.

[69] S. Srinivasan, et al., Role of mitochondrial reactive oxygen species in osteoclast differentiation, Ann. N. Y. Acad. Sci. 1192 (2010) 245–252, https://doi.org/10.1111/j.1749-6632.2009.05377.x.